UNDERSTANDING THE NONLINEAR BEHAVIOUR AND SYNCHRONIZING STABILITY OF A GRID-TIED VSC UNDER GRID VOLTAGE SAGS

Chen Zhang[1*], Marta Molinas[1], Jing Lyu[2], Haoxiang Zong[2], Xu Cai[2]

[1] Department of Engineering Cybernetics of Norwegian University of Science and Technology, Trondheim, Norway

[2]Department of Electrical Engineering of Shanghai Jiao Tong University, Shanghai, China

**chen.zhang@ntnu.no*

Keywords: TRANSIENT, STABILITY, NONLINEAR, SYNCHRONIZATION, VSC

Abstract

Transients of a typical grid synchronizing VSC are closely associated with the over-current and over-voltage in circuits. Previous analysis in evaluating such transient phenomenon usually ignore the nonlinear control effects of the VSCs (e.g. phase-locked-loop, PLL). Although this assumption allows a simpler analysis of the transient process, it may overlook potential stability issues on which the nonlinear controls may a great impact and the consequence of which is easily confused with the passive circuit transients. Therefore, this work aims to achieve a good understanding of the nonlinear control dynamics of the VSC and their impacts on the stability provoked by the grid voltage sags. To better reveal the mechanisms, the power control loop (PCL) and the PLL-dominant dynamics are analysed separately with corresponding reduced-order nonlinear models. From which the grid synchronizing stability of the VSC is revealed, and a quantitative study of stability margin is presented through the calculation and evaluation of the critical clearing time (CCT). Based on this, CCT under various PLL bandwidths are evaluated, the results of which could facilitate the parameter design of PLL from a stability viewpoint. All the analyses are verified by time-domain simulations in PSCAD/EMTDC.

1 Introduction

Voltage source converters (VSCs) are widely adopted in integrating renewable energy power generations (e.g. wind and solar power) with AC grid [1], as well as in interconnecting two asynchronous grids via the high-voltage-dc (HVDC) technology [2].

Despite its fast and flexible power control capability, recent experience shows that VSCs are susceptible to oscillate against a weak AC grid, e.g. a case of wind farm case in [3] and photovoltaic plant in [4], where the nonlinear dynamics of the phase-locked-loop (PLL) have drawn great attention. To explain and analyze these oscillation behaviors, efforts have been made (e.g. [5] and [6]), however in a small signal sense due to the consideration that most of the oscillations occurred are caused by a moderate change of system configurations. This allows linear-based methods to identify and predict the forward behavior around a steady state operating point. In this regard, many methods are applicable, and among which the impedance-based method becomes popular since the impedance can be either analytically modelled or practically measured.

Impedance models of a typical three-phase VSC can be in different formats according to the linearization methods employed. Typically, linearizing in sequence domain [7] results in a sequence impedance (e.g. [8] and [9]), whereas linearizing in *dq* domain [10] yields a *dq* impedance (e.g. [11] and [12]). Recently, other modeling methods, e.g. a phasor-based [13], a modified sequence domain based [14], a single-input and single-output based [15] and a complex transfer function based [16] methods are available, in which the properties of converters can be explained more intuitively, e.g. the mirror coupling effects [14] originated from the *dq* asymmetry of impedance matrices [17]. Despite different modeling techniques, all these models are capable of identifying oscillatory behaviors in a grid-tied VSC system by applying Nyquist-based stability analysis [18]. A useful finding is that PLL is of great importance for VSC small signal stability, particularly under a weak AC grid condition (e.g. [11] and [19]). Moreover, behaviors of PLL can be physically interpreted as a current-controlled-voltage-source (CCVS) in an equivalent RLC circuit of VSC-grid system [20], where the CCVS can exhibit negative damping to the equivalent RLC circuit if conditions in are met.

However, above discussions are conducted in the linear domain which can only predict the dynamics around a steady-state operating point, if the oscillation diverges, the subsequent behavior can no longer be predicted accurately, e.g. a limit cycle. In [21], a large signal impedance model is proposed to study the sustained oscillations, where the PWM saturation is properly modeled compared to the typical impedance model, e.g. [11]. In [22] and [23], a state space nonlinear model of VSC is proposed, where the bifurcation phenomenon is observed. However, these analyses focus on the memoryless nonlinearities (e.g. saturation), where the dynamical nonlinearities (e.g. PLL) are not discussed.

One step further, a phasor-based analysis of a wind farm with grid voltage dips are studied in [24] and [25], where the wind farm model is simplified to a current source. Requirements on the limitation of active current injection, in the presence of grid voltage dips are emphasized. This work provides an important implication that the current injection of VSC may lead to angle stability from a steady-state point of view. [26] moves further in this regard, where the same conclusion is drawn from the positive feedback effects of the PLL. Although [24]-[26] lack of a dynamical analysis, they are helpful and illuminated in reconsidering the origin of the VSC's transients and its potential stability impact.

To bridge this gap, this paper aims to achieve a fundamental understanding of the nonlinear behavior of a typical VSC and its potential consequences on stability, all the transients are provoked by the grid voltage sags. This paper is organized as follows, in section 2, the nonlinear behavior of the power control loop (PCL) is analyzed firstly, where the PLL is assumed steady. Then, the PLL- dominant nonlinear behavior is explored in section 3, where the grid synchronizing stability (GSS) is identified and the mechanism of which is revealed. Based on the developed mechanism, stability margin of GSS is quantitatively evaluated through the calculation of the critical clearing time (CCT). Section 4 draws the main conclusion.

2. Analysis of the PCL dominant nonlinear dynamics

2.1 Description of the study system

Fig. 1 illustrates a typical grid-tied VSC, which is composed of a current control loop (CCL), a PCL and a PLL (H_c, H_s, H_{pll} are their PI controllers respectively). Usually, the VSC is connected to the bulk grid via two step-up transformers (T_1 and T_2) to boost voltage to the transmission level, hence the "equivalent grid" seen from the VSC (i.e. at the point of

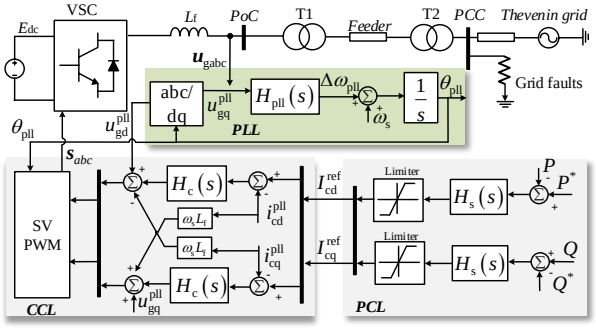

Fig. 1 Schematic of a typical grid connected VSC system

connection, PoC) is relatively weak, even though the impedance of the Thevenin grid (i.e. impedance seen from the point of common coupling, PCC) is small. This weak grid condition can lead to oscillation if the dynamics of the PLL and CCL are not decoupled in terms of time-scale, this small-signal-stability issue has been extensively studied in the literature as discussed before, e.g., in [20]. This work, therefore, assumes a properly designed CCL, which means CCL is much faster than PLL and PCL. Therefore, the CCL is assumed in a quasi-steady state if dynamics in the time scale of the PLL or PCL are analysed.

Table 1 Main parameters

Symbol	Name	Value
S_n	rating/base	2 MW
U_n	nominal/base voltage	690 V
V_{dc}	dc voltage	1200 V
f_{sw}	switching frequency	2.4 kHz
f_s	fundamental frequency	50 Hz
L_f	filter inductance	$7.6\text{x}10^{-5}$ H
L_T	Leakage inductance of $T_{1,2}$	0.1 p.u.

2.2 Modelling of the PCL dominant dynamics

Model reduction is necessary to allow an analytical study of nonlinear behaviours of a complex system. This section aims to analyse the PCL dominant dynamics, hence PLL is assumed steady temporarily. Based on this assumption, the voltage equation from the PoC ($\boldsymbol{U}_g^{pll}$) to the Thevenin grid voltage ($\boldsymbol{U}_s^{pll}$) can be written as:

$$\boldsymbol{U}_g^{pll} = j\omega_{pll} L_\Sigma \boldsymbol{I}_c^{pll} + \boldsymbol{U}_s^{pll} \tag{1}$$

where, the output currents ($\boldsymbol{I}_c^{pll}$) of VSC are assumed steady due to their fast dynamics, i.e. $\boldsymbol{I}_c^{pll} \approx \boldsymbol{I}_c^{ref}$. All the vectors are projected to the PLL reference frame (denoted by superscript 'pll'). Since the PLL is assumed steady in this case, $\omega_{pll} = \omega_s$ is imposed. In PLL fame, the Thevenin grid voltage can be represented as: $\boldsymbol{U}_s^{pll} = U_s \cos\theta_0 - jU_s \sin\theta_0$, where θ_0 is the steady angle difference between U_g and U_s. L_Σ is the lumped system inductance seen from PoC, it can be quantified by the short circuit ratio (SCR), i.e. in per unit format $\bar{L}_\Sigma$=1/SCR. The output power of VSC in complex format is:

$$\begin{aligned} &P + jQ = \boldsymbol{U}_{pcc}^{pll}\left(\boldsymbol{I}_c^{pll}\right)^* = j\omega_{pll} L_\Sigma \left|\boldsymbol{I}_c^{pll}\right|^2 + \boldsymbol{U}_s^{pll}\left(\boldsymbol{I}_c^{pll}\right)^* \rightarrow \\ &\begin{cases} P = U_s \cos\theta_0 \cdot I_{cd} - U_s \sin\theta_0 \cdot I_{cq} \\ Q = \omega_s L_\Sigma \left(I_{cd}^2 + I_{cq}^2\right) - \left(U_s \cos\theta_0 I_{cq} + U_s \sin\theta_0 I_{cd}\right) \end{cases} \end{aligned} \tag{2}$$

It can be observed from (2) that the active power P is a linear combination of the dq currents, whereas the reactive power Q is not. Next, the dynamical equation of PCL can be further derived from the control blocks in Fig. 1 as:

$$\begin{cases} \dfrac{dx_d}{dt} = k_i\left(P^* - P\right) \\ \dfrac{dx_q}{dt} = k_i\left(Q^* - Q\right) \\ I_{cd} = x_d + k_p\left(P^* - P\right) \\ I_{cq} = -x_q - k_p\left(Q^* - Q\right) \end{cases} \tag{3}$$

In which, x_d, x_q are the output states of PI integrators, while k_p and k_i are PI parameters of H_s. Consequently, (2) and (3) consist of the model of PCL-dominant dynamics.

2.3 Nonlinear behaviour analysis

Due to the developed PCL model is of second-order, phase portraits can, therefore, be adopted to study nonlinear its behaviours. In Fig.2, current phase portraits with varying PQ controller (H_s) parameters are plotted.

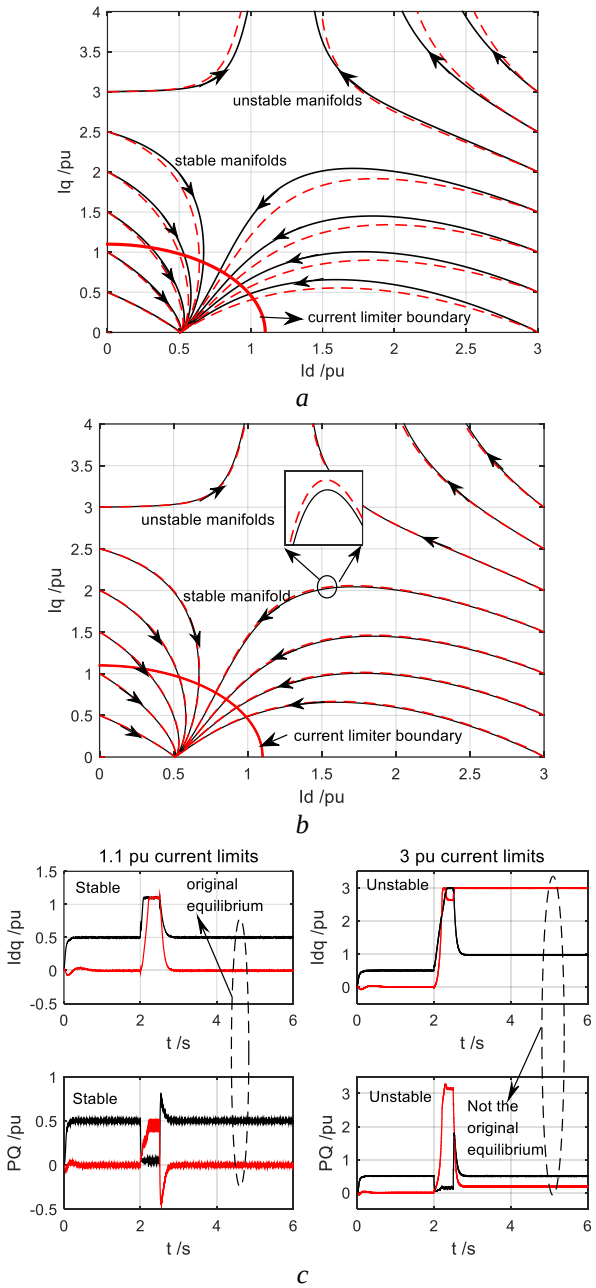

Fig.2 (a) Phase portraits with varying k_p, P = 0.5 pu, Q = 0 pu, SCR = 4 (solid line k_p = 0.1, dotted line k_p = 0.2); (b) Phase portraits with varying k_i , P = 0.5 pu, Q = 0 pu, SCR = 4 (solid line k_i = 20, dotted line k_i = 40); (c) Time domain simulations, k_p = 0.1, k_i = 20 (black lines: I_d/P, red lines denote I_q/Q)

From Fig.2 (a) one could observe that the states (I_{cd} , I_{cq}) can be either attracted by the stable manifolds or driven away by the unstable manifolds, depending on their initial values. In other words, the equilibrium (0.5, 0) in this case has a limited region of attraction, consequently, any initial states that are close enough to the equilibrium can be attracted, otherwise a divergent of states can occur. On the other side, comparing the dotted line and solid line we can identify that, increasing the proportional gain of PQ controller (H_s) has a negative impacts on stability (i.e. region of attraction becomes smaller), whereas the integral gain has negligible effects on the phase portraits as depicted in Fig.2 (b).

To validate the analysis, time domain simulations are presented in Fig.2 (c), where the transient responses of currents (I_{dq}) and active/reactive power (P/Q) under a symmetrical grid fault are measured. In accordance with the model assumption, PLL frequency is locked to 1.0 p.u. after VSC is synchronized (i.e. at 1.8s). As shown in Fig.2 (c), if the currents are limited to a relatively small value (left columns), the system can converge to the original equilibrium (i.e. (Id, Iq) = (0.5, 0)) after grid fault is cleared, this case is consistent with the analysis in Fig.2 (a) with initial states within the region of attraction.

However, if the currents are limited to a relatively large value (right column in Fig.2 (c)), the system cannot converge to its original equilibrium but to another "steady" point. It should be noted that this "steady" point is not an equilibrium because the reactive power does not converge to its set-point, which is Q = 0. Hence, a condition: $\dot{x}_d = 0, \dot{x}_q \neq 0$ can be obtained from (3). Further based on (2) we can notice that, it has three unknowns (i.e. Q, I_d, I_q) but only with two independent equations, thus the solution is not unique, and the "steady" point shown in Fig.2 (c) (right column) is essentially one of them. Apparently, this steady point is not an equilibrium since the condition $\dot{x}_d = 0, \dot{x}_q = 0$ is not satisfied.

Another finding should be addressed is that, although the theoretical analysis can be unstable, this may be unachievable due to the current limits in practice should be small for protection purpose (e.g. typical values are Imax = 1.1), therefore, all the initial states of currents can be constrained in the region of attraction (red arcs in Fig.2 (a) and (b)), which means the nonlinear dynamics of the PCL could be absolute stable under such practical constraints.

3. Analysis of the PLL dominant nonlinear dynamics

Previous section analysed the PCL dominant nonlinear behaviours, where the PLL is assumed steady. In this section, for better revealing the GSS, the nonlinear behaviour of PLL-dominant dynamics will be analysed in detail, likewise, a slow regulation of the PCL is assumed, thus the current reference of the CCL is assumed constant.

3.1 Modelling of PLL dominant dynamics

Based on the above assumption, in the time-scale of PLL dynamics, $\boldsymbol{I}_{\mathrm{c}}^{\mathrm{pll}} \approx \boldsymbol{I}_{\mathrm{c}}^{\mathrm{ref}}$ is imposed, i.e. a fast CCL and $\boldsymbol{I}_{\mathrm{c}}^{\mathrm{ref}}$ remains steady due to the assumption of a slow PCL.

Then, the input of PLL is the q axis voltage at PoC, i.e. $u_{\mathrm{gq}}^{\mathrm{pll}} = \mathrm{Im}\left\{\boldsymbol{u}_{\mathrm{g}}^{\mathrm{pll}}\right\}$ from (1). In combination with PLL control blocks in Fig. 1, the following equations can be obtained:

$$\begin{cases} \dfrac{d\Delta\omega_{\mathrm{pll}}}{dt} = k_{\mathrm{p}}^{\mathrm{pll}} \cdot \dot{u}_{\mathrm{gq}}^{\mathrm{pll}} + k_{\mathrm{i}}^{\mathrm{pll}} u_{\mathrm{gq}}^{\mathrm{pll}} \\ \dfrac{d\delta_{\mathrm{pll}}}{dt} = \Delta\omega_{\mathrm{pll}} \end{cases} \tag{4}$$

In which, $u_{\mathrm{gq}}^{\mathrm{pll}} = \omega_{\mathrm{pll}} L_{\Sigma} I_{\mathrm{cd}}^{\mathrm{ref}} - U_{\mathrm{s}} \sin\delta_{\mathrm{pll}}$, $\delta_{\mathrm{pll}} = \theta_{\mathrm{pll}} - \theta_{\mathrm{s}}$. $k_{\mathrm{p}}^{\mathrm{pll}}$ and $k_{\mathrm{i}}^{\mathrm{pll}}$ are the PI parameters of H_{pll}. In the later analysis, PLL bandwidth (α_{pll}) is frequently used instead of PI parameters, in which $k_{\mathrm{p}}^{\mathrm{pll}} = 2\alpha_{\mathrm{pll}} / \mathrm{U_s}$ and $k_{\mathrm{i}}^{\mathrm{pll}} = 2\alpha_{\mathrm{pll}}^2 / \mathrm{U_s}$ are adopted [20].

Converting (4) into per unit format, yields:

$$\begin{cases} T_{\mathrm{pll}} \dfrac{d\Delta\bar{\omega}_{\mathrm{pll}}}{dt} = -D_{\mathrm{pll}}\Delta\bar{\omega}_{\mathrm{pll}} + \bar{T}_{\mathrm{m}} - \bar{T}_{\mathrm{e}} \\ \dfrac{d\delta_{\mathrm{pll}}}{dt} = \omega_{\mathrm{b}}\Delta\bar{\omega}_{\mathrm{pll}} \\ D_{\mathrm{pll}}\left(\delta_{\mathrm{pll}}\right) = \dfrac{k_{\mathrm{p}}^{\mathrm{pll}}}{k_{\mathrm{i}}^{\mathrm{pll}}}\left(\bar{U}_{\mathrm{s}} \cos\delta_{\mathrm{pll}} \omega_{\mathrm{b}} - \bar{L}_{\Sigma}\bar{I}_{\mathrm{cd}}^{\mathrm{ref}}\right) \\ T_{\mathrm{pll}} = \dfrac{\omega_{\mathrm{b}} - k_{\mathrm{p}}^{\mathrm{pll}}\bar{L}_{\Sigma}\bar{I}_{\mathrm{cd}}^{\mathrm{ref}}}{k_{\mathrm{i}}^{\mathrm{pll}}} \\ \bar{T}_{\mathrm{m}} = \bar{\omega}_{\mathrm{s}}\bar{L}_{\Sigma}\bar{I}_{\mathrm{cd}}^{\mathrm{ref}}, \bar{T}_{\mathrm{e}} = \bar{U}_{\mathrm{s}} \sin\delta_{\mathrm{pll}} \end{cases} \tag{5}$$

where ω_{b} is the base value of the angular frequency. T_{pll} is a constant, whereas D_{pll} is δ_{pll} dependent. For a small value of δ_{pll}, $D_{\mathrm{pll}}\left(\delta_{\mathrm{pll}}\right)$ is positive; otherwise, it can be negative. $\bar{T}_{\mathrm{m}}$ is constant input, $\bar{T}_{\mathrm{e}}$ is the nonlinear state feedback to the frequency dynamics.

Consequently, the nonlinear model of PLL-dominant dynamics is developed in (5). One may observe that this model resembles the motion equation of a synchronous generator (SG), which means the well-known SG-based transient angle analysis methods are applicable, e.g. the equal area principle (EAP). Due to this similarity, the variable notation of an SG is adopted to the definition of the variables of the PLL dynamics, e.g. $\bar{T}_{\mathrm{m}}$, $\bar{T}_{\mathrm{e}}$, though $\bar{T}_{\mathrm{m}}$ and $\bar{T}_{\mathrm{e}}$ are essentially voltages in physics.

3.2 Nonlinear Behaviour analysis

Similar to the analysis of the PCL dominant dynamics, the PLL dominant dynamics is characterized as a second-order nonlinear system as well, e.g., (5), rendering a graphical analysis of dynamical behaviours through the phase portrait, where $\left(\Delta\bar{\omega}_{\mathrm{pll}}, \delta_{\mathrm{pll}}\right)$ are the two state variables.

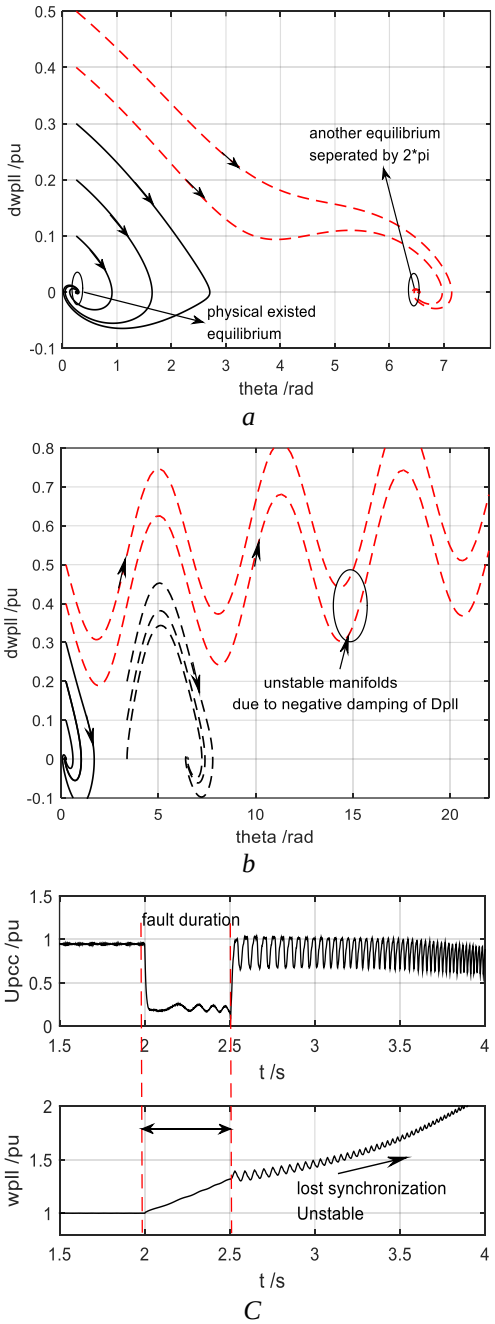

Fig. 3 (a) D_{pll} approximated by a constant at δ_{pll0}; (b) D_{pll} varies with angle δ_{pll}; (c) Time domain simulations; PLL bandwidth is 20 Hz, i.e. $k_{\mathrm{p}}^{\mathrm{pll}} = 20$, $k_{\mathrm{i}}^{\mathrm{pll}} = 800$, SCR = 4, $\bar{I}_{\mathrm{cd}}^{\mathrm{ref}} = 1$ pu; in (c), a symmetrical grid fault is applied at PCC with a duration of 500ms

First, in Fig. 3 (a), the phase portraits of (5) with varying initial states $\left(\Delta\omega_{\mathrm{pll0}}, \delta_{\mathrm{pll0}}\right)$ are plotted, where the damping term is approximated by a positive constant $D_{\mathrm{pll}}\left(\delta_{\mathrm{pll0}}\right)$ (i.e. evaluated at δ_{pll0}). One could observe that for small initial

states, the state trajectory can converge to the original point after several cycles' motion. However, if the initial states are far away from this point, they can converge as well, but to another equilibrium that separated by 2π. This is an intrinsic property of the nonlinear system (5) that, there is an equilibrium set (i.e. $\delta_{\text{pll0}}+2k\pi$, $k=\pm1,\pm2...$) that is locally stable, and states can always converge to the equilibrium set due to $D_{\text{pll}}\left(\delta_{\text{pll0}}\right)$.

Further, as emphasized before, the damping term D_{pll} is a nonlinear function of δ_{pll}, which means it can be negative if δ_{pll} is large (e.g. $\delta_{\text{pll}}\in\left[2k\pi+\frac{\pi}{2},2k\pi+\frac{3\pi}{2}\right],k=0,\pm1...$). Therefore, a detailed phase portrait including the effects of $D_{\text{pll}}\left(\delta_{\text{pll}}\right)$ is plotted in Fig. 3 (b). Clearly, the system can be unstable (see the dotted and red line) if the initial states $\left(\Delta\omega_{\text{pll}},\delta_{\text{pll}}\right)$ are large. This feature cannot be captured by Fig. 3 (a) since the approximated constant $D_{\text{pll}}\left(\delta_{\text{pll0}}\right)$ is positive.

A time domain simulation is conducted and presented in Fig. 3 (c), where the PLL frequency and the magnitude of PCC voltage are measured. In order to have a large deviation of initial states, a symmetrical grid fault is applied at PCC with a duration of 500ms, it can be clearly identified that the PLL lost synchronization after the grid fault is cleared, and it exhibits a similar manner as the phase portrait in Fig. 3 (b).

3.3 Mechanism analysis of the GSS

As mentioned before, the EAP for the transient stability analysis of an SG [27] can be applied to the analysis of PLL dominant dynamics due to the resemblance.

According to (5), characteristics of $\bar{T}_{\text{m}}=\bar{\omega}_{\text{s}}\bar{L}_{\Sigma}\bar{I}_{\text{cd}}^{\text{ref}}$ and $\bar{T}_{\text{e}}=\bar{U}_{\text{s}}\sin\delta_{\text{pll}}$ can be illustrated by curves in Fig. 4 (a). It can be observed that a grid fault can change the characteristic of $\bar{T}_{\text{e}}$ abruptly, whereas $\bar{T}_{\text{m}}$ remains constant (i.e. $\bar{T}_{\text{m}}^{0+}=\bar{T}_{\text{m}}^{0-}$) due to the current is assumed steady. The magnitude differences between $\bar{T}_{\text{e}}^{0+}$ and $\bar{T}_{\text{m}}^{0+}$ can result in the acceleration of system states: $\left(\Delta\omega_{\text{pll}},\delta_{\text{pll}}\right)$. Then, after a short period, the grid fault is cleared (e.g. at point C), where characteristic curve of $\bar{T}_{\text{e}}^{0+}$ changes back to its pre-fault value ($\bar{T}_{\text{e}}^{0-}$), so that $\Delta\omega_{\text{pll}}$ starts decelerating due to $\bar{T}_{\text{e}}^{0-}$ is greater than $\bar{T}_{\text{m}}^{0-}$. However, δ_{pll} will remain increasing until $\Delta\omega_{\text{pll}}$ becomes zero again.

The EAP claims that if $\exists S_{\text{II}}\left(\Delta\omega_{\text{pll}}=0,\delta_{\text{pll}}\le\delta_{\text{pll}}^{\text{B}}\right):S_{\text{I}}=S_{\text{II}}$, then the system is referred to as first swing stable. It should be noted that, although the nonlinear system (5) can converge to an equilibrium set (e.g. in Fig. 3 (a)) as discussed before, only the principal one i.e., $\Delta\omega_{\text{pll}}=0,\delta_{\text{pll}}=\delta_{\text{pll0}}$ is of interests or physical significance. Because the transition from one equilibrium to another can exhibit large transients in currents or voltages, which are not allowed due to the limited stress of physical components. For an SG, this also indicates a "pole slip" operation, which is detrimental and not allowed.

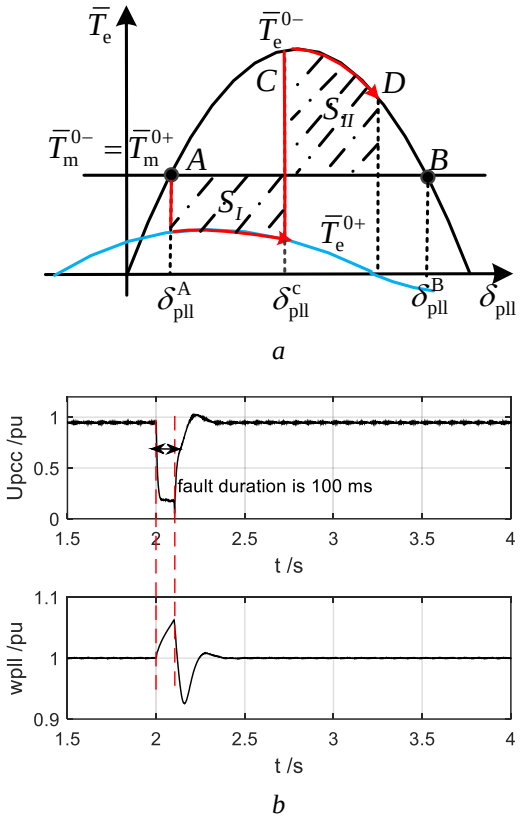

Fig. 4 (a) EAP-based mechanism analysis (Superscript "0-" and "0+" denote pre-fault and post-fault; point A is pre-fault equilibrium, point C is fault clearing point); (b) Time domain simulations (conditions are the same as Fig. 3 (c), except that fault duration is reduced to 100ms).

From the EAP it is obtained that, if the fault clearing angle $\delta_{\text{pll}}^{\text{C}}$ is small (i.e. fault is cleared fast), then there is more margin for the deceleration area that stability can be assured. To illustrate this character, a time domain simulation is shown in Fig. 4 (b), where the fault is cleared faster compared to the one in Fig. 3 (c). Clearly, the frequency of PLL is stable under such a condition, indicating that a small $\delta_{\text{pll}}^{\text{C}}$ is helpful for stability.

Based on the above analysis, it is seen that the fault clearing angle can be a metric of the GSS margin. Specificlly, the critical condition that ensuring a first swing stable system is of most interest, i.e. there exists a critical angle that EAP is met, i.e. $\exists\delta_{\text{pll}}^{\text{CCA}}:S_{\text{I}}=S_{\text{II}}^{\max}\left(\Delta\omega_{\text{pll}}=0,\delta_{\text{pll}}^{\max}=\delta_{\text{pll}}^{\text{B}}\right)$. This angle is referred to as Critical Clearing Angle (CCA), its calculation will be shown subsequently.

3.4 Analysis of the GSS margin

The CCA can be calculated by numerical method if the analytical model of $\bar{T}_e^{0+}$, $\bar{T}_e^{0-}$ and $\bar{T}_m$ are known, in which $\bar{T}_e^{0-}$ and $\bar{T}_m$ can be obtained from (5), whereas $\bar{T}_e^{0+}$ is fault dependent.

To calculate the post-fault $\bar{T}_e^{0+}$, circuit analysis of the grid fault is necessary. In accordance with PLL modelling, the equivalent circuit of Fig.1 can be drawn in Fig. 5 (a), where $\boldsymbol{Z}_{\Sigma T}$ is the lumped line impedance seen from PoC, $\boldsymbol{Z}_S$ is the source impedance seen from PCC, $\boldsymbol{Z}_f$ is the short circuit impedance applied at PCC.

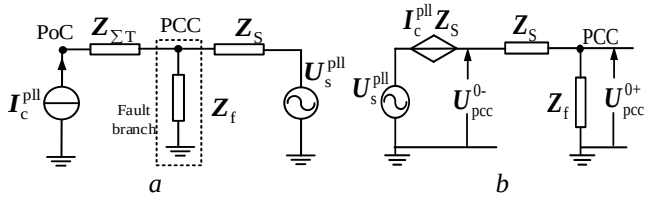

Fig. 5 (a) Equivalent circuit of Fig. 1; (b) Post-fault circuit

A Thevenin equivalent circuit seen from the fault branch can be further developed in Fig. 5 (b), in which the post-fault PCC voltage can be calculated as: $\boldsymbol{U}_{pcc}^{0+} = \boldsymbol{k}_f \cdot \boldsymbol{U}_{pcc}^{0-}$, where $\boldsymbol{U}_{pcc}^{0-} = \boldsymbol{U}_s^{pll} + \boldsymbol{I}_c^{pll}\boldsymbol{Z}_s$ and $\boldsymbol{k}_f = \boldsymbol{Z}_f / (\boldsymbol{Z}_f + \boldsymbol{Z}_s) = k_f e^{j\varphi_f}$.

Therefore, the post-fault characteristic of $\bar{T}_e^{0+}$ is obtained:

$$\bar{T}_e^{0+} = \mathrm{Im}\left\{\boldsymbol{U}_{pcc}^{0+}\right\} = k_f U_{pcc}^{0-} \sin\left(\delta_{pll} - \varphi_f\right) \tag{6}$$

where, $\delta_{pll} = \theta_{pll} - \theta_{pcc}$ is redefined, meanwhile $\bar{T}_e^{0-}$ in (5) is modified to $\bar{T}_e^{0-} = U_{pcc}^{0-} \sin\delta_{pll}$, and $\bar{T}_m$ is modified to $\bar{T}_m = \bar{\omega}_s \bar{L}_{\Sigma T} \bar{I}_{cd}^{ref} + \bar{R}_{\Sigma T} \bar{I}_{cq}^{ref} \approx \bar{\omega}_s \bar{L}_{\Sigma T} \bar{I}_{cd}^{ref}$.

From (6) it is observed that, in geometry, $\bar{T}_e^{0+}$ is essentially a curve deformation of $\bar{T}_e^{0-}$, consequently $\bar{T}_e^{0+}$ can be easily drawn in Fig. 4 (a) by shifting and compressing curve $\bar{T}_e^{0-}$. As the grid impedance $\boldsymbol{Z}_s$ is mostly inductive, and if $\boldsymbol{Z}_f$ is inductive as well, there exhibits no phase shift according to the expression of $\boldsymbol{k}_f$ (i.e. $\varphi_f = 0$). Otherwise, for a resistive short circuit branch, the phase shift can be $\varphi_f \in \left(-\frac{\pi}{2}, 0\right)$. Usually, effects of φ_f is negligible since the acceleration and deceleration areas (S_I and S_{II}) are primarily determined by the magnitude of $\bar{T}_e^{0+}$, particularly under severe grid sags.

Based on the models of $\bar{T}_e^{0+}$, $\bar{T}_e^{0-}$ and $\bar{T}_m$, the CCA can be calculated numerically from the nonlinear algebraic equation:

$$S_I = S_{II}^{max} \rightarrow \int_{\delta_{pll}^A}^{\delta_{pll}^{CCA}} \left(\bar{T}_m - \bar{T}_e^{0+}\right) d\delta_{pll} = -\int_{\delta_{pll}^{CCA}}^{\delta_{pll}^B} \left(\bar{T}_m - \bar{T}_e^{0-}\right) d\delta_{pll} \tag{7}$$

If resubstituting the numerical results of CCA into the dynamical equation of $\Delta\omega_{pll}$ in (5), the corresponding Critical Clearing Time (CCT) can be estimated as:

$$t_{CCT} = \frac{\left(\delta_{pll}^{CCA} - \delta_{pll}^{A}\right)}{k_0} \sqrt{\frac{T_{pll}}{2S_I\omega_b}} \tag{8}$$

where k_0 is a coefficient that used to estimate the integral of $\int_0^{t_{CCT}} \omega_b \Delta\omega_{pll} dt$ by $\left(k_0 \omega_b \Delta\omega_{pll}^C\right) \cdot t_{CCT}$, in this work $k_0 = 2/3$ is adopted. The CCT is a more intuitive metric since the time can be more easily measured than the CCA.

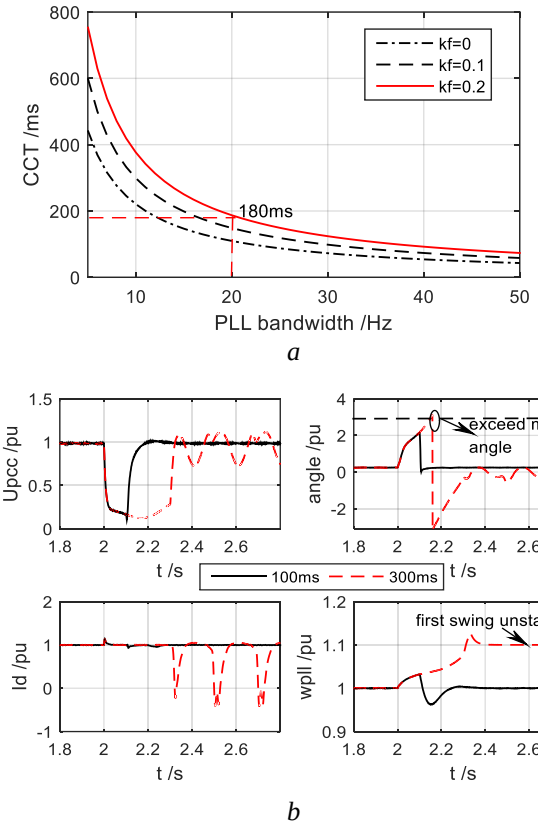

Fig. 6 (a) CCT with varying PLL bandwidth (SCR = 4, $\bar{L}_{\Sigma T} = 0.2$ pu, $\bar{I}_{cd}^{ref} = 1$ pu, $\varphi_f = 0$); (b) Time domain simulations (a symmetrical grid fault is applied at 2s, the maximum angle denotes $\delta_{pll}^B = \pi - \delta_{pll}^A \approx 3$ rad, $\delta_{pll}^A = 0.253$ rad, a frequency limiter for PLL is at 1.1 pu)

To illustrate the feasibility of CCT in evaluating stability margin, a numerical evaluation of the CCT with varying PLL bandwidth is conducted and the results are plotted in Fig. 6 (a). It is seen that by increasing the PLL bandwidth, the CCTs are reducing, which means stability margin is deteriorated. On the other hand, the magnitudes of $\bar{T}_e^{0+}$ (i.e.

voltage dips at PCC) can also affect CCT to some extends, but its effects can be limited if PLL bandwidth is large.

To further address the validity of the numerical analysis, a time domain simulation is conducted in Fig. 6 (b). In which, a 20 Hz PLL bandwidth is selected, where we can find from Fig. 6 (a) that the CCT = 180ms, which means the system is stable if the fault is cleared at a duration less than this CCT value. Therefore, a100ms (<CCT) and a 300ms (>CCT) fault clearing time are compared in simulations. It is shown in Fig. 6 (b) that, for the case of 100ms fault duration, the system is stable after fault is cleared (solid black lines). However, for a 300ms fault duration, the system is unstable after grid fault is cleared (dotted red lines), proving the numerical stability analysis is correct.

Furthermore, from the current waveform (Fig. 6 (b)) one may further observe that the current assumption made in PLL time-scale is feasible due to it can remain steady despite the varying of PLL frequency in the fault period. And, from the angle waveform, it is further observed that the angle for the unstable case exceeds the maximum allowed angle (i.e. δ_{pll}^{B} in Fig. 4 (a)) in the fault period, resembling the first swing unstable of an SG.

4 Conclusion

Recent endeavors have shown than VSC controls may actively involve in transients caused by large grid disturbances, e.g. voltage sags, in which the nonlinear dynamics may be provoked and the effects of which should not be overlooked. To achieve a fundamental understanding of the VSC's nonlinear behaviours and their stability impacts, this paper analysed the nonlinear behaviours of the PCL and the PLL separately, the principle enabling this separated study is the well-known multi-time scale property of a dynamical system.

Based on this methodology, the nonlinear dynamics of PCL is first analysed, although the PCL could theoretically lead to instability, it turns out that if the practical constraints are considered (e.g. limitation of currents above the nominal value), the PCL can be regarded as stable from a practical point of view. Therefore, the focuses are put on the PLL dominant dynamics.

In this regard, as revealed in this work, the PLL exhibits a similar nonlinear behaviour as the SG's swing dynamics, which may lead to grid-synchronizing stability issue under certain conditions (e.g. a large grid fault with a fast PLL). One major difference from the analysis of an SG is that the PLL dynamics may exhibit negative damping if the angle deviation is large. If limit the stability to a first swing cycle, a small angle deviation assumption can be imposed, and this allows a quantitative study of the stability margin through the calculation of the CCT. In this regard, a detailed derivation and calculation of CCT are presented, and evaluation of CCT with varying PLL bandwidths is conducted to show how the PLL parameters affect grid synchronizing stability.

This numerical calculation of CCT can also be employed for studying the stability impacts of other parameters, e.g. the phase jump of grid voltage.

5 Acknowledgements

This work is support in part by NTNU energy under Grant 81617922 and in part by the National Natural Science Foundation of China under Grant 51837007

6 References

[1] Teodorescu R, Liserre M, Rodriguez P. "Introduction," in Grid converters for photovoltaic and wind power systems. Chichester, United Kingdom: John Wiley & Sons, 2011, pp:1-4.

[2] Flourentzou N, Agelidis V G, Demetriades G D. "VSC-Based HVDC Power Transmission Systems: An Overview," IEEE Trans. Power Electron, vol.24, no.3, pp.592-602, 2009.

[3] Liu, H., Xie, X., He, J., Xu, T., Yu, Z., Wang, C., & Zhang, C. (2017). Subsynchronous interaction between direct-drive PMSG based wind farms and weak AC networks. IEEE Transactions on Power Systems, 32(6), 4708-4720.

[4] C. Li, "Unstable Operation of Photovoltaic Inverter from Field Experiences," in IEEE Trans. Power Del, doi: 10.1109/TPWRD.2017.2656020.

[5] Kunjumuhammed, L. P, et al. "Electrical Oscillations in Wind Farm Systems: Analysis and Insight Based on Detailed Modeling," IEEE Transactions on Sustainable Energy, pp.1-12, 2015.

[6] Yang D, Ruan X, Wu H. "Impedance Shaping of the Grid-Connected Inverter with LCL Filter to Improve Its Adaptability to the Weak Grid Condition," IEEE Trans. Power Electron, vol.29, no.11, pp.5795-5805, 2014.

[7] Sun J, "Small-Signal Methods for AC Distributed Power Systems–A Review," in IEEE ESTS., Baltimore, Maryland, 2009, pp.44-52.

[8] Cespedes M, Sun J. "Impedance Modeling and Analysis of Grid-Connected Voltage-Source Converters," IEEE Trans. Power Electron, vol.29, no. 3, pp.1254-1261, 2014.

[9] Bakhshizadeh, Mohammad Kazem, et al, "Couplings in Phase Domain Impedance Modeling of Grid-Connected Converters," IEEE Trans. Power Electron, vol.31, no.10, pp.6792-6796, 2016.

[10] M. Belkhayat, "Stability criteria for AC power systems with regulated loads". Purdue University, USA, 1997.

[11] Wen, Bo, et al. "Small-Signal Stability Analysis of Three-Phase AC Systems in the Presence of Constant Power Loads Based on Measured d-q, Frame

Impedances," IEEE Trans. Power Electron, vol.30, no.10, pp.5952-5963, 2015.

[12] Harnefors L, Bongiorno M, Lundberg S. "Input-Admittance Calculation and Shaping for Controlled Voltage-Source Converters," IEEE Trans. Ind. Electronics, vol.54, no.6, pp.3323-3334, 2007

[13] Shah, S., & Parsa, L. (2017). Impedance modeling of three-phase voltage source converters in dq, sequence, and phasor domains. IEEE Transactions on Energy Conversion, 32(3), 1139-1150.

[14] Rygg, A., Molinas, M., Zhang, C., & Cai, X. (2016). A modified sequence-domain impedance definition and its equivalence to the dq-domain impedance definition for the stability analysis of AC power electronic systems. IEEE Journal of Emerging and Selected Topics in Power Electronics, 4(4), 1383-1396.

[15] Zhang, C., Cai, X., Rygg, A., & Molinas, M. (2017). Sequence domain siso equivalent models of a grid-tied voltage source converter system for small-signal stability analysis. IEEE Transactions on Energy Conversion.

[16] Wang X, Harnefors L, Blaabjerg F, PC Loh. "A Unified Impedance Model of Voltage-Source Converters with Phase-Locked Loop Effect," IEEE ECCE, United States, 2016.

[17] Harnefors, L. (2007). Modeling of three-phase dynamic systems using complex transfer functions and transfer matrices. IEEE Transactions on Industrial Electronics, 54(4), 2239-2248.

[18] Sun J. "Impedance-Based Stability Criterion for Grid-Connected Inverters," IEEE Trans. Power Electron, vol.26, no. 11, pp. 3075-3078, 2011.

[19] Dong D, Wen B, Boroyevich D, et al. "Analysis of phase-locked loop low-frequency stability in three-phase grid-connected power converters considering impedance interactions," IEEE Trans. Ind. Electron, vol.62, no. 1, pp.310-321, 2015

[20] Zhang, C., Cai, X., Li, Z., Rygg, A., & Molinas, M. (2017). Properties and physical interpretation of the dynamic interactions between voltage source converters and grid: electrical oscillation and its stability control. IET Power Electronics, 10(8), 894-902.

[21] S. Shah and L. Parsa, "Large-signal impedance for the analysis of sustained resonance in grid-connected converters," 2017 IEEE 18th Workshop on Control and Modeling for Power Electronics (COMPEL), Stanford, CA, 2017, pp. 1-8

[22] M. Huang, Y. Peng, C. K. Tse, Y. Liu, J. Sun and X. Zha, "Bifurcation and Large-Signal Stability Analysis of Three-Phase Voltage Source Converter Under Grid Voltage Dips," in IEEE Transactions on Power Electronics, vol. 32, no. 11, pp. 8868-8879, Nov. 2017.

[23] M. Huang, H. Ji, J. Sun, L. Wei and X. Zha, "Bifurcation-Based Stability Analysis of Photovoltaic-Battery Hybrid Power System," in IEEE Journal of Emerging and Selected Topics in Power Electronics, vol. 5, no. 3, pp. 1055-1067, Sept. 2017.

[24] I. Erlich, F. Shewarega, S. Engelhardt, J. Kretschmann, J. Fortmann and F. Koch, "Effect of wind turbine output current during faults on grid voltage and the transient stability of wind parks," 2009 IEEE Power & Energy Society General Meeting, Calgary, AB, 2009, pp. 1-8.

[25] Martínez, Jorge, et al. "Active current control in wind power plants during grid faults." Wind Energy 13.8(2015):737-749.

[26] Ö. Göksu, R. Teodorescu, C. L. Bak, F. Iov and P. C. Kjær, "Instability of Wind Turbine Converters During Current Injection to Low Voltage Grid Faults and PLL Frequency Based Stability Solution," in IEEE Transactions on Power Systems, vol. 29, no. 4, pp. 1683-1691, July 2014.

[27] P. Kundur et al., "Definition and classification of power system stability IEEE/CIGRE joint task force on stability terms and definitions," in IEEE Transactions on Power Systems, vol. 19, no. 3, pp. 1387-1401, Aug. 2004.